IEEE Access
Multidisciplinary | Rapid Review | Open Access Journal

Received 9 September 2023, accepted 24 September 2023, date of publication 4 October 2023, date of current version 11 October 2023.

Digital Object Identifier 10.1109/ACCESS.2023.3322006

RESEARCH ARTICLE

Effect of Faulty Solenoid Starter on the DC Series Motor Performance in Railway Industry

SOHEIL YOUSEFNEJAD[1], EBRAHIM AMIRI[2], (Senior Member, IEEE), MOHSEN SARPARAST[3], AND JONG-SUK RO[4,5], (Member, IEEE)

[1]Electrical Engineering Department, The University of New Orleans, New Orleans, LA 70148, USA
[2]Electrical Engineering Department, California State University Long Beach, Long Beach, CA 90840, USA
[3]Department of Mechanical, Industrial and Manufacturing Engineering, The University of Toledo, Toledo, OH 43606, USA
[4]School of Electrical and Electronics Engineering, Chung-Ang University, Seoul 06974, South Korea
[5]Department of Intelligent Energy and Industry (BK4), Chung-Ang University, Seoul 06974, South Korea

Corresponding author: Jong-Suk Ro (jongsukro@gmail.com)

ABSTRACT Cranking railway engines in high currents could lead to a series of undesirable effects on the starter motor such as melting copper contacts and disk inside the solenoid. This paper investigates the impact of a defective solenoid on the performance of a DC series motor starter. First, the effect of the starting system on the solenoid parts (i.e., the melting phenomenon in copper contacts and disk inside the solenoid) is described via Finite Element (FE). Next, the circuit model of the DC series motor with the solenoid starter is established to obtain the motor performance. Results reveal that subjecting the contactor disk to a current of 1250 A for 30 *ms* would melt the disk and cause surface defects. The faulty/melted disk subsequently raises the circuit resistance to 2.9 m ohms. The presented solution can detect the faults effect within 0.05 *s* time frame. Simulation results are supported via a series of experimental measurements and detailed theoretical discussion.

INDEX TERMS Fault detection, DC series motor, starter solenoid, railway industry.

NOMENCLATURE

$q_w(r)$	Plasma heat flux.
F_c	Fraction of discharge power.
V	Breakdown voltage.
I	current.
R	Plasma channel.
r	Radial position.
V_{dc}	Voltage across the motor winding.
R_{dc}	Motor DC resistance.
W_r	Speed of the motor.
L_{af}	Coefficient of the motor.
I_a	Motor current.
L_{au}	Total inductance of the motor.
L_{AA}	Inductance of the armature.
L_{ff}	Inductance of the motor field.
R_a	Resistance of the armature.
R_f	Resistance of the motor field.
T_e	Electrical torque of the motor.
T_L	Mechanical torque of the motor.
B	Damping coefficient.
R_t	Total resistance of motor set.
L_t	Total inductance of the motor.
R_s	Resistance of the series path of the motor.
L_s	Inductance of the series path of the motor.

The associate editor coordinating the review of this manuscript and approving it for publication was Akshay Kumar Saha.

I. INTRODUCTION

Brush-type DC series motor has been a popular choice for starting diesel engines in transportation/railway industry, thanks to its high initial/starting torque [1], [2], and easy control mechanism [3], [4], [5]. However, cranking such a system in high currents could lead to a series of undesired-able effects such as melting in copper contacts and disk inside the solenoid (which behaves like a switch for the starter system). Documented literature includes various solutions to improve the cranking mechanism, and thus to limit the damage [6]. Examples include adding an additional supercapacitor in the circuit of the DC series motor and battery to increase the

cranking speed [7], using a supercapacitor instead of the battery [8], and improvement of storage system/battery reliability [9] and diesel engine start-ability [10]. However, the best remedy may directly come from the solenoid structure [11], [12], and/or the electric motor structure itself [13], [14].

While the previous studies have addressed the thermal aspects [12] and Electro-dynamical modeling [15] of a solenoid coil, this research fills an important gap by considering disk and contactors as a critical component within the solenoid starter that can influence its functionality.

Motivated by the important role of the solenoid starter in the railway industry, and in the absence of a comprehensive research in condition monitoring of solenoid's contacts/disk, this paper aims to identify and investigate the effect of the faulty solenoid on the DC series motor performance. First, the thermal effect of electric discharge and spark (due to the passage of high current through the solenoid) inside the solenoid is described and obtained via Finite Element (FE). Next, the circuit model of the DC series motor with the solenoid starter is established to investigate the effect of the faulty solenoid on the DC series motor performance (e.g., motor speed, motor current). For further confirmation, simulated results are verified by a series of experimental tests.

This paper is organized as follows. Section II discusses the structural description of the solenoid starter. Section III presents the circuit model of the solenoid starter and describes the thermal effect of the electric discharge inside the solenoid. Section IV presents results, discussion, and experimental tests, followed by concluding remarks in Section V.

II. STRUCTURAL DESCRIPTION AND OPERATING PRINCIPLE

DC series motors equipped with solenoid starter are commonly used in railway industry for cranking the engine [15]. The starter motor has a pinion that meshes with the teeth on the engine's flywheel and turns the crankshaft. It supplies power to the motor through the battery. As the ignition switch is turned on, the solenoid gets energized. By exciting the hold-in and pull-in coils of the solenoid, the disk and contacts are engaged, and thus, the current of the DC series motor flows through the contacts and the disk. Next, the contacts and the disk complete the circuit from the battery to the motor and apply the voltage of the battery to the terminal of the motor and cause the rotor to spin. Due to the high current demand of the motor, the ignition switch needs to be relatively large to handle such high current level. However, the surface of the disk and the contactor may erode over time and therefore, a lower amount of current is transmitted to the electric motor. This may disrupt the process of exerting torque to the crankshaft, and thereby the ignition of the engine. The schematic of the starter solenoid, DC series motor and related circuit are shown in Fig. 1 and Fig. 2, respectively.

III. ELECTRIC DISCHARGE AND MODELING PROCEDURE

Electric discharge deformation is an electro-thermal process that occurs by discrete and repetitive electrical sparks

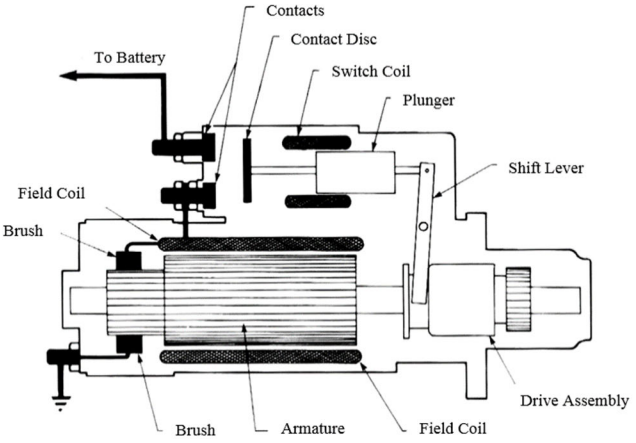

FIGURE 1. Structure of the starter solenoid and DC series motor [18].

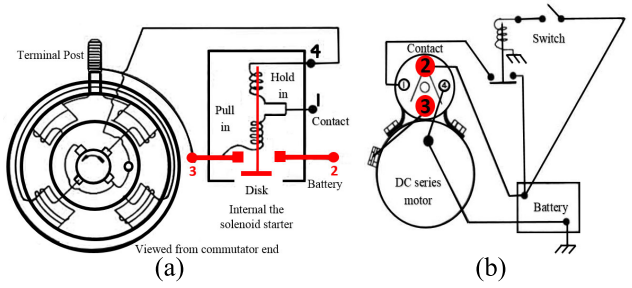

FIGURE 2. Schematic of the solenoid starter and DC series motor (a) internal wiring (b) external wiring [18].

between two electrodes separated by a small distance. The high temperature plasma channel causes local melting and vaporization and erodes tiny amount of materials from the work surface [16]. To conduct a thermo-physical analysis of a single spark operation between connectors during current discharge a Gaussian-distributed heat flux [17] with sufficient boundary condition is utilized in FE.

A. HEAT FLUX

The effective amount of heat rate entering the workpiece converted to thermal energy and absorbed by the workpiece. Relation (1) presents the heat flux as a function of radius via Gaussian distribution during electric discharging [16]:

$$q_w(r) = \frac{4.57F_cVI}{\pi R^2} e^{-4.5(\frac{r}{R})^2} \quad (1)$$

Due to high-temperature gradients during discharging, several thermo-physical properties such as specific heat, density, and thermal conductivity shall be considered. Since the electro-discharge analysis process is an intricate and complicated, the following assumptions are considered to simplify the process:

- workpieces are assumed isotropic and homogeneous.
- Only one spark happens during each pulse (single spark).
- All the materials the temperature is over than melting temperature are assumed to be eliminated by the dielectric rush upon the collapse of the plasma channel.

Numerical models and analyses of single spark discharge process are exceedingly helpful to clarify the shape of the spark region. Thus, to simulate the varying temperature of two pieces of contactors, a 3-D model is developed in a commercially available FE software package. Given the symmetrical structure of the contactor switch and disk, only a portion of the structure (between the contactor and disk in the discharge spark region with an effective area of 19.2 mm^2) is modeled.

Non-uniform Gaussian distribution of heat flux is coded, and linked to the FE software, and the heat flux value is calculated at discrete time instants via subroutine DFLUX. Table 1 summarizes the most important parameters used for the FE thermal analysis of a typical single spark electric-discharging process, and Table 2 shows thermo-physical properties variable of the copper material. The FE thermal analysis is implemented based on the algorithm of Fig. 3.

Fig. 4 presents the simulated temperature profile of the disk and identifies the region(s) that their temperature exceeds the melting point (i.e., 1084 °C) of the contacts and disk material. Fig 4 illustrates that disk surface experiences very high temperature (up to about 1.104 × 103 °C as the maximum temperature) at the early stages of discharge, which occurs at the center of plasma channel due to the nature of Gaussian flux distribution. This temperature is clearly above the melting point and even vaporizing point of the disk and connector surface. Meanwhile, the molten boundary obtained by eliminating all the elements whose temperatures exceeded 1084°C (the melting point of copper), spreads only to a small volume of material.

B. ELECTRICAL MODEL

The circuit diagram of the DC series motor with the solenoid starter is shown in Fig. 5, and is described by the following set of relations [19]:

$$V_{dc} = \left(R_{dc} + W_r L_{af}\right) I_a + L_{au}\left(\frac{dI_a}{dt}\right) \quad (2)$$

$$R_{dc} = R_a + R_f \quad (3)$$

$$L_{au} = L_{AA} + L_{ff} \quad (4)$$

$$T_e - T_L = j\left(\frac{dW_r}{dt}\right) + BW_r \quad (5)$$

$$T_e = L_{af} I_a^2 \quad (6)$$

$$V_t = \left(R_t + W_r L_{af}\right) I_a + L_t\left(\frac{dI_a}{dt}\right) \quad (7)$$

$$R_t = R_{dc} + R_s \quad (8)$$

$$L_t = L_{au} + L_s \quad (9)$$

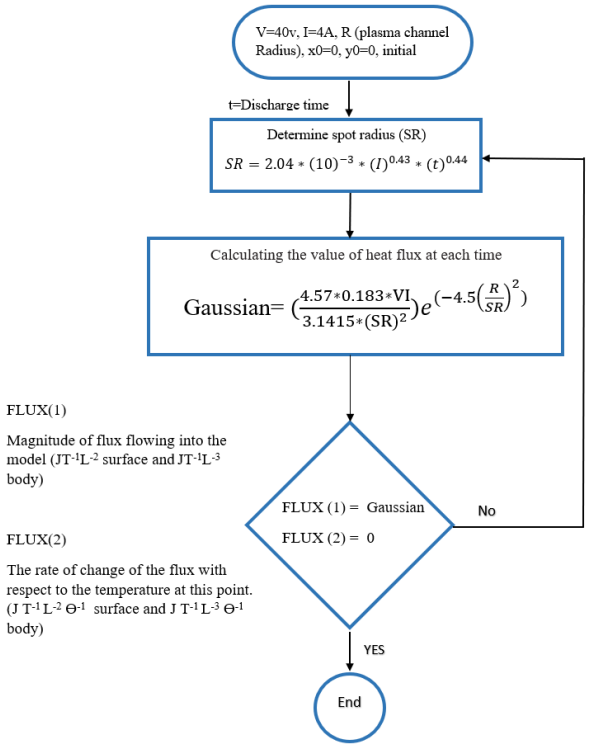

FIGURE 3. Step-by-step FE thermal analysis.

TABLE 1. Parameters used for a typical single discharge FE simulation.

Type of Element	4-node thermally coupled quadrilateral
Solution method	Iterative Newton–Raphson
Time step	Fixed
Meshing type	Structured meshing
Discharge Current (A)	1250
Spark on-time (μs)	30
Discharge voltage (V)	26.4

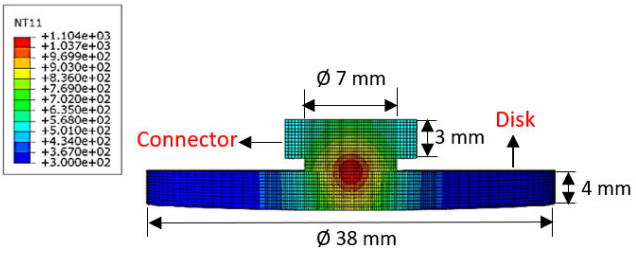

FIGURE 4. Temperature distribution contours for t = Tdis = 30 ms, I = 1250 A and Vdis = 26.4V.

IV. RESULTS, DISCUSSION AND EXPERIMENTAL VALIDATION

The main nameplate data of the motor start are listed in Table 3. The experimental testbed of the motor start (DC series motor and solenoid) is shown in Fig. 6. A shunt resistor is placed in series with the motor start to measure the current via a current measuring unit (Ammeter). Speed is measured by using an encoder with a pulse rate of 100 pulses per revolution and a data logger (NI USB-6009). Sampling time is adjusted 10000 per second. The acquired speed data were subsequently analyzed using computer-based techniques, with a moving average approach [21]. the moving

TABLE 2. Temperature-dependent thermo-physical properties of copper used in simulations [20].

Temperature [k]	Specific heat [J/kgk]	Conductivity [w/mk]	Density ρ (kg/m3)	Temperature [k]	Specific heat [J/kgk]	Conductivity [w/mk]	Density ρ (kg/m3)
300	112	400	8962	1500	445	161	7881
400	147	393	8910	1600	446	164	7799
500	180	385	8872	1700	456	168	7717
600	209	378	8824	1800	467	170	7635
700	237	372	8763	1900	477	174	7553
800	261	367	8711	2000	485	175	7471
900	288	358	8652	2100	489	178	7389
1000	316	351	8581	2200	494	177	7307
1100	362	344	8513	2300	498	178	7225
1200	405	338	8446	2400	503	180	7143
1300	448	331	8375	2500	507	181	7098
1400	449	160	7962	2600	505	181	7085

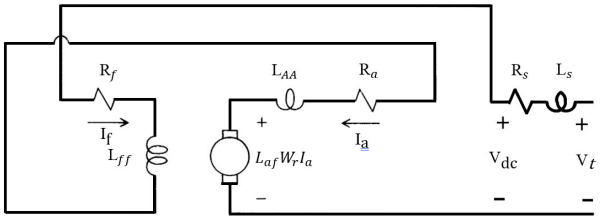

FIGURE 5. DC series motor circuit with solenoid starter and all joints.

TABLE 3. Design parameters of the test bench.

Parameter	Value
Manufacturer	LEECE NEVILLE
Model	Prestolite MS7-501A
Weight (Kg)	29.5000
Voltage	24 V
Power	9.0 kW
Pinion Teeth	11
Rotation Direction	CW
Notes	Oil-sealed. Rotatable nose

average of order m follows as:

$$T_t = \frac{1}{m}\sum_{j=-k}^{k} y_{t+j} \tag{10}$$

$$m = 2k + 1 \tag{11}$$

where y is data, m is the order of moving average, k is the periods of t, and t is time.

The melted disk and contacts may form a coarse and irregular surface depending upon extent/degree of which disk and contacts are melted. This decreases the effective contact area and thereby, increases the resistance. As a result, the current drops since the solenoid windings and battery voltage remain the same in both faulty and healthy conditions [22], [23]. In other words, the resistance of faulty solenoid is higher than the healthy ones. Although, faulty solenoid has a lower inductance value as discussed in section IV.

When the solenoid is energized, the disk gets pushed toward the contacts. When the disk and contacts are connected, the disk will hold into contacts. The contacts and disk are made of copper and are capable of carrying currents beyond 1300 Amperes. As illustrated in Fig. 7, the spark formed at the switching instant melts the disk surface. To determine the level of damage/erosions the resistance of the disk and contacts is measured by milliohm-meter, indicating the resistance rising up by over 2.9 milli-ohm. This increases the voltage drop and there-by, lowers the motor's terminal voltage and subsequently the motor speed. In extreme scenarios, the speed of the motor and therefore, the flywheel speed may not reach the desired level necessary to start the diesel engine. For illustration purposes, the healthy and faulty disk and contacts are shown in Fig 8. The motor parameters at faulty and healthy conditions are presented in Table 4.

The profile of the motor current and speed at faulty and healthy conditions are measured and compared against simulated results in Fig. 9.

As seen, the motor current reaches to a table state after 1.5 s, justifying the decision to conduct all experiments within a 1.5 s interval, although, the faulty disk diagnosis is done within the first 50-millisecond timeframe.

To investigate the effects of motor parameters on the speed and current profile, sensitivity analysis is carried out in terms

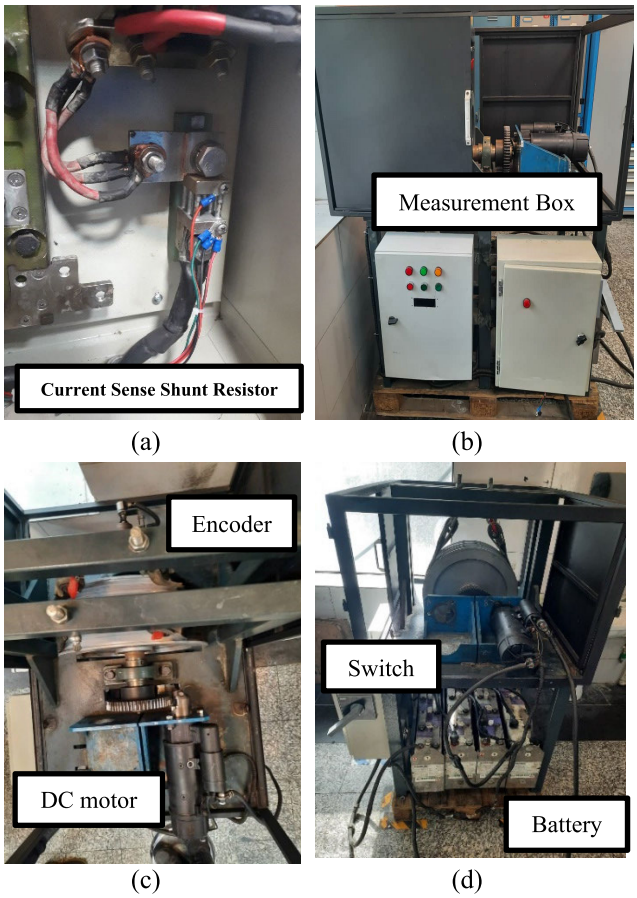

FIGURE 6. Test bench of the motor start.

FIGURE 7. After a couple of attempts at switching the motor start.

of total resistance (R_t) and total inductance of the motor (L_t) and inductance of the armature (L_{af}) (Figs. 10-12). As seen, the crest point of the current curve is delayed at higher inductance values.

Finally, to investigate the impact of faulty solenoid, the profile of current and speed at faulty conditions are measured and compared against healthy condition in Fig 13.

As seen in Fig. 13(a), the faulty solenoid operates at a lower speed due to higher resistance in the circuit. Also, the motor current, and therefore the motor torque drops below the healthy levels. As a result, the generated torque may not be sufficient to rotate the flywheel at the desired speed, and thereby complete the cranking process. The speed drop in and of itself is an indicative of a faulty system.

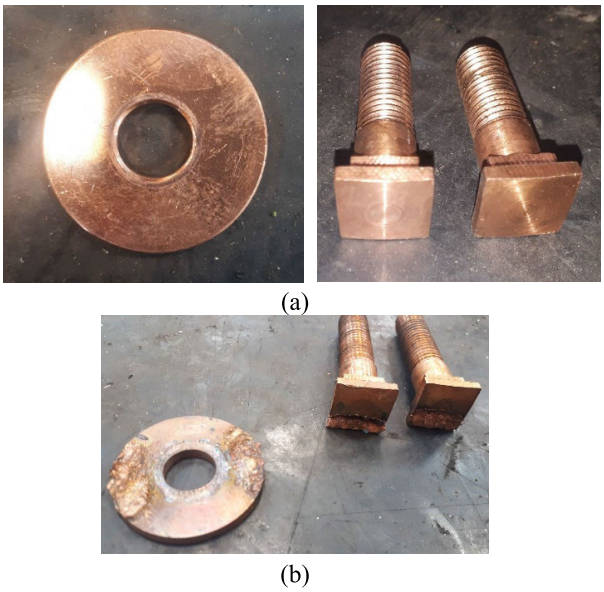

FIGURE 8. Disk and contacts in solenoid starter of dc series motor. (a) healthy condition (b) faulty condition.

TABLE 4. Motor parameters.

	Healthy (TB0)	Fault1 (TB1)	Fault2 (TB2)
R_s^* (mΩ)	0.8	2	2.2
R_t^{**}(mΩ)	8.3	9.5	9.7
L_{af}^{***} (μH)	26.5	27	28
L_t^{****}(μH)	395	325	310
j	0.0086	0.0086	0.0086
Stall torque	47	49	53

* Resistance of the series path of the motor, ** total resistance, *** Inductance of the armature, **** Inductance of the motor

Also, Fig.13(b) indicates that the crest of current curve is shifted toward left similar to the pattern shown in Fig. 12. This implies that the faulty solenoid lowers the inductance L_t.

V. VALIDATION OF THE PARAMETERS OF THE SOLENOID IN DC SERIES MOTOR

In this section the effect of the faulty solenoid is shown analytically. Before the motor start reaches to the certain speed, the motor start draws high current and this current feeds by the battery. In this moment based on the instrument in the last section, the battery voltage for healthy and faulty solenoid kept the same. because from first to 30 *ms* in the cranking step, the speed is less than 35 rpm in this motor and L_{af} is less than 500 μH. So, it is acceptable to ignore the following term.

$$W_r L_{af} I_a \approx 0 \tag{12}$$

And

$$V_{battery} = (R_t)\, I_a + L_t \left(\frac{dI_a}{dt}\right) \tag{13}$$

Then, in the 0<t<0.03, as it is shown in the instruments, the current of the healthy and malfunctioning solenoid is

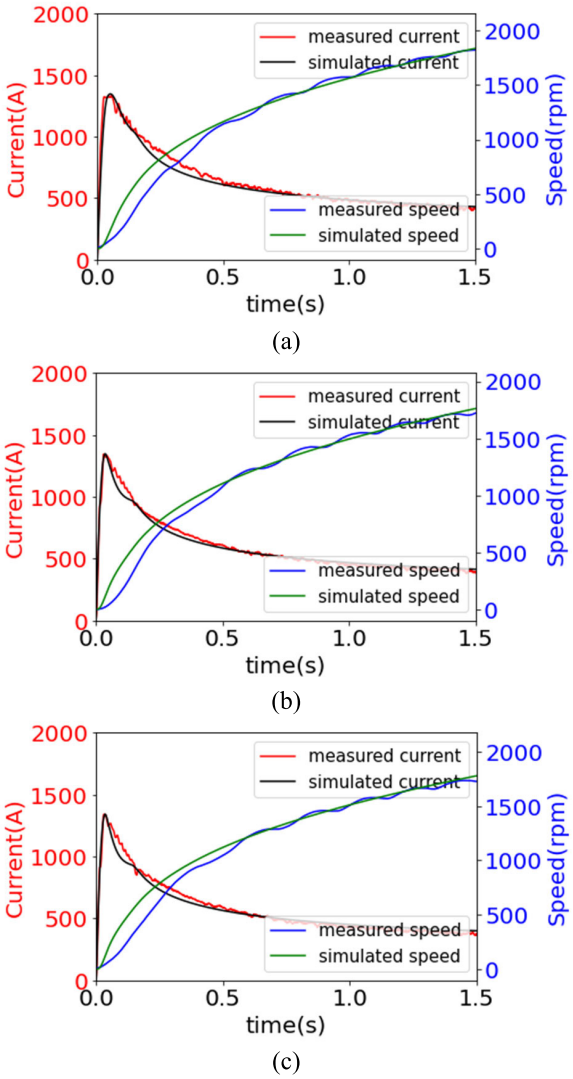

FIGURE 9. The profile of motor speed and motor current (measured and simulated) (a) healthy solenoid starter (TB0), (b) faulty solenoid starter (TB1), and (c) faulty solenoid starter (TB2).

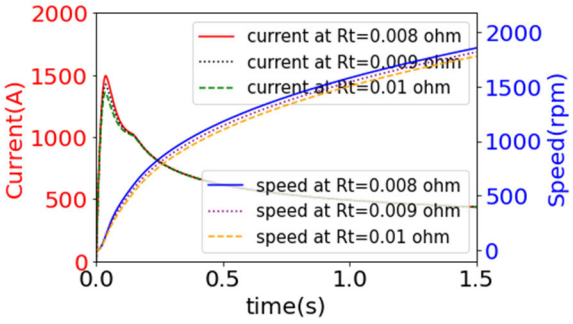

FIGURE 10. Effect of increasing Rt on speed and current.

nearly identical.

$$I_{a\_F} \approx I_{a\_H} \approx I_a \tag{14}$$

$$\left(R_{t\_F} - R_{t\_H}\right) I_a = \left(L_{t\_H} - L_{t\_F}\right) \left(\frac{dI_a}{dt}\right) \tag{15}$$

As it is discussed, because the resistance of the faulty solenoid is increased, the inductance of the current path in

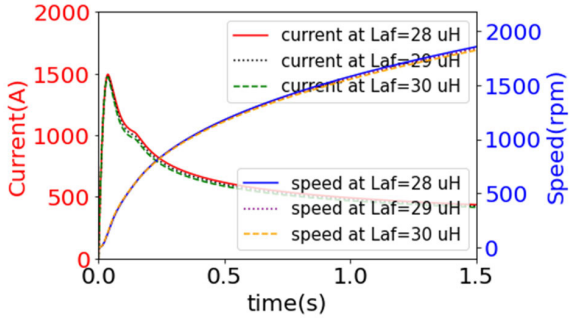

FIGURE 11. Effect of increasing L_{af} on speed and current.

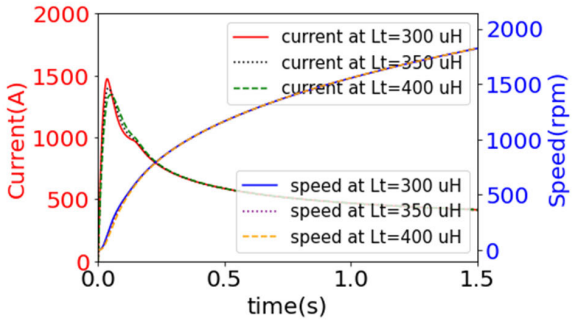

FIGURE 12. Effect of increasing L_t on speed and current.

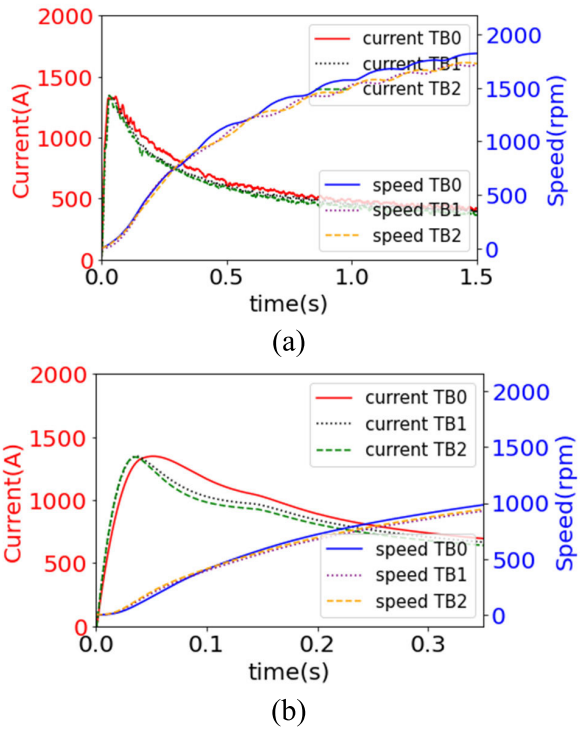

FIGURE 13. The current and speed of the healthy and the faulty DC series motor (b) in the start point.

the motor start with the faulty solenoid is decreased in comparison with healthy one.

VI. CONCLUSION

In this paper, the reasons for melting in the disks and contacts of the solenoid in DC series motors used in the railway industry, small ships, and automotive industries are

explained in detail. The role of the disk and contactors as crucial components within the solenoid starter is highlighted, and the primary source of fault is explained. Because cranking/starting diesel engine with a solenoid starter would demand a very high current, it could melt the disk and cause surface defects. The DC series motor and solenoid are modeled, simulated, and validated with experimental tests. Results revealed that subjecting the contactor disk to a current of 1250 A for 30 *ms* would melt the disk and cause surface defects. The faulty or melted disk subsequently increases the circuit resistance to 2.9 milliohms, depending on the overall condition of the engine, motor start, and battery.

REFERENCES

[1] S. Arof, N. M. Noor, M. F. Alias, E. Noorsal, P. Mawby, and H. Arof, "Digital proportional integral derivative (PID) controller for closed-loop direct current control of an electric vehicle traction tuned using pole placement," in *Progress in Engineering Technology II*. Cham, Switzerland: Springer, 2020, pp. 73–89, doi: 10.1007/978-3-030-46036-5_8.

[2] S. Lu, Y. Qin, J. Hang, B. Zhang, and Q. Wang, "Adaptively estimating rotation speed from DC motor current ripple for order tracking and fault diagnosis," *IEEE Trans. Instrum. Meas.*, vol. 68, no. 3, pp. 741–753, Mar. 2019.

[3] G. Shultz, *Transformers and Motors*. Amsterdam, The Netherlands: Elsevier, 2012.

[4] L. Hao, C. S. Namuduri, S. Gopalakrishnan, C. J. Lee, N. S. Shidore, M. Pandi, and T. Vandermeir, "Brushless fast starter for automotive engine start/stop application," *IEEE Trans. Ind. Appl.*, vol. 56, no. 6, pp. 6041–6052, Nov. 2020.

[5] M. Hajiaghajani, H. A. Toliyat, and I. M. S. Panahi, "Advanced fault diagnosis of a DC motor," *IEEE Trans. Energy Convers.*, vol. 19, no. 1, pp. 60–65, Mar. 2004.

[6] W. M. H. R. Wickramasinghe, K. T. G. M. Duleeka, H. D. Kolamunna, and S. G. Abeyratne, "A power electronics assisted emergency vehicle starter," in *Proc. 16th Int. Power Electron. Motion Control Conf. Expo.*, Sep. 2014, pp. 283–288.

[7] H. Liu, Z. Wang, J. Cheng, and D. Maly, "Improvement on the cold cranking capacity of commercial vehicle by using supercapacitor and lead-acid battery hybrid," *IEEE Trans. Veh. Technol.*, vol. 58, no. 3, pp. 1097–1105, Mar. 2009.

[8] V. L. Kokate, P. B. Karandikar, A. Kumari, D. Kaira, and R. Rai, "Innovative approach for increasing reliability in electronic cranking in two wheelers," in *Proc. Int. Conf. Circuit, Power Comput. Technol. (ICCPCT)*, Apr. 2017, pp. 1–6.

[9] C. Boccaletti, S. Elia, E. F. Salas M, and M. Pasquali, "High reliability storage systems for genset cranking," *J. Energy Storage*, vol. 29, Jun. 2020, Art. no. 101336.

[10] A. Celik, M. Yilmaz, and O. F. Yildiz, "Improvement of diesel engine startability under low temperatures by vortex tubes," *Energy Rep.*, vol. 6, pp. 17–27, Nov. 2020.

[11] S. Z. A. S. K. Bahrin and U. A. U. Amirulddin, "Design and development of a new electromagnetic prime mover using solenoid technology solenoid powered engine model simulation (torque vs. speed characteristic)," in *Proc. IEEE Int. Conf. Power Energy (PECon)*, Dec. 2014, pp. 255–259.

[12] J. Li, M. Xiao, Y. Sun, G. Nie, Y. Chen, and X. Tang, "Failure mechanism study of direct action solenoid valve based on thermal-structure finite element model," *IEEE Access*, vol. 8, pp. 58357–58368, 2020.

[13] V. M. Murugesan, R. Rudramoorthy, G. Chandramohan, M. Senthil Kumar, L. Ashok Kumar, K. Vishnu Murthy, and R. S. Kumar, "Development of ECU based starting system for automobiles," in *Proc. Int. Conf. Process Autom., Control Comput.*, Jul. 2011, pp. 1–5.

[14] M. A. Koondhar, A. A. Malak, M. A. Koondhar, and I. A. Channa, "Experimental based comparative analysis and characteristics of DC series motor by using different techniques," *Sukkur IBA J. Emerg. Technol.*, vol. 3, no. 1, pp. 2616–7069, Jul. 2020.

[15] L. Nagy, T. Szabó, and E. Jakab, "Electro-dynamical modeling of a solenoid switch of starter motors," *Proc. Eng.*, vol. 48, pp. 445–452, Dec. 2012.

[16] C. Sanghani, G. Acharya, and K. D. Kothari, "A simulation-based approach for modelling of fraction of energy transfer to workpiece in electrical discharge machining," *Int. J. Manuf. Res.*, vol. 15, no. 3, pp. 285–296, May 2020.

[17] S. Assarzadeh and M. Ghoreishi, "Electro-thermal-based finite element simulation and experimental validation of material removal in static gap single-spark die-sinking electro-discharge machining process," *Proc. Inst. Mech. Eng., B, J. Eng. Manuf.*, vol. 231, no. 1, pp. 28–47, Jan. 2017.

[18] Prestolite. (1985). *Prestolite Maintenance Publication for Aircraft Engines*. Novi, MI, USA. [Online]. Available: https://www.csobeech.com/files/PrestoliteStarterAlternatorManual.pdf

[19] S. J. Chapman, *Electric Machinery Fundamentals*. New York, NY, USA: McGraw-Hill, 2004.

[20] M. A. Attar, M. Ghoreishi, and Z. M. Beiranvand, "Prediction of weld geometry, temperature contour and strain distribution in disk laser welding of dissimilar joining between copper & 304 stainless steel," *Optik*, vol. 219, Oct. 2020, Art. no. 165288.

[21] R. J. Hyndman and G. Athanasopoulos, *Forecasting: Principles and Practice*. Melbourne, VIC, Australia: OTexts, 2018.

[22] E. Dullni, D. Gentsch, W. Shang, and T. Delachaux, "Resistance increase of vacuum interrupters due to high-current interruptions," *IEEE Trans. Dielectr. Electr. Insul.*, vol. 23, no. 1, pp. 1–7, Feb. 2016.

[23] G. Wu, J. Wu, W. Wei, Y. Zhou, Z. Yang, and G. Gao, "Characteristics of the sliding electric contact of pantograph/contact wire systems in electric railways," *Energies*, vol. 11, no. 1, p. 17, Dec. 2017.

SOHEIL YOUSEFNEJAD received the B.S. degree in electrical engineering and in electrical power engineering from Shahid Beheshti University, Tehran, Iran, in 2015, and the M.Sc. degree in electrical power engineering from the Iran University of Science and Technology (IUST), Tehran, in 2018. He is currently pursuing the Ph.D. degree in electrical engineering with The University of New Orleans, New Orleans, LA, USA. His research interests include magnetic gears and electrical machines design and lithium-ion battery charger.

EBRAHIM AMIRI (Senior Member, IEEE) received the B.Sc. and M.Sc. degrees in electrical engineering from the Amirkabir University of Technology, Tehran, Iran, in 2005 and 2008, respectively, and the Ph.D. degree in electrical engineering from Louisiana State University, Baton Rouge, LA, USA, in 2013. In January 2015, he joined the Electrical and Computer Engineering Department, The University of New Orleans, where he was a Graduate Program Coordinator (2020–2023) and the Chair of the Department (2022–2023). In July 2023, he joined the Electrical Engineering Department, California State University Long Beach. His current research interests include design, development, and modeling of electric machines.

MOHSEN SARPARAST received the B.S. degree in mechanical engineering from the Babol Noshirvani University of Technology, in 2014, and the M.S. degree in mechanical engineering from the K. N. Toosi University of Technology, Iran, in 2018. He is currently pursuing the Ph.D. degree in mechanical engineering with The University of Toledo, OH, USA. His research interests include the manufacturing process, computational modeling, and machine learning.

JONG-SUK RO (Member, IEEE) received the B.S. degree in mechanical engineering from Hanyang University, Seoul, South Korea, in 2001, and the Ph.D. degree in electrical engineering from Seoul National University (SNU), Seoul, in 2008. In 2014, he was with the University of Bath, Bath, U.K., as an Academic Visitor. From 2013 to 2016, he was with the Brain Korea 21 Plus, SNU, as a BK Assistant Professor. He conducted research with the Electrical Energy Conversion System Research Division, Korea Electrical Engineering and Science Research Institute, as a Researcher, in 2013. From 2012 to 2013, he was with the Brain Korea 21 Information Technology, SNU, as a Postdoctoral Fellow. He conducted research with the Research and Development Center, Samsung Electronics, as a Senior Engineer, from 2008 to 2012. He is currently an Associate Professor with the School of Electrical and Electronics Engineering and an Adjunct Professor with the Department of Intelligent Energy and Industry (BK4), Chung-Ang University, Seoul. His research interests include the analysis and optimal design of next-generation electrical machines using smart materials, such as electromagnet, piezoelectric, and magnetic shape memory alloy.